Energies **2014**, *7*, 4710-4726; doi:10.3390/en7074710

OPEN ACCESS

energies

ISSN 1996-1073

www.mdpi.com/journal/energies

Article

Research on Cellular Instabilities of Lean Premixed Syngas Flames under Various Hydrogen Fractions Using a Constant Volume Vessel

Hong-Meng Li, Guo-Xiu Li *, Zuo-Yu Sun, Yue Zhai and Zi-Hang Zhou

School of Mechanical, Electronic and Control Engineering, Beijing Jiaotong University, Beijing 100044, China; E-Mails: 11116350@bjtu.edu.cn (H.-M.L.); sunzy@bjtu.edu.cn (Z.-Y.S.); zhaiyue0000@163.com (Y.Z.); Zhou_zihang@yahoo.com (Z.-H.Z.)

* Author to whom correspondence should be addressed; E-Mail: Li_guoxiu@yahoo.com; Tel./Fax: +86-10-5168-3684.

Received: 2 April 2014; in revised form: 10 July 2014 / Accepted: 15 July 2014 / Published: 22 July 2014

Abstract: An experimental study of the intrinsic instabilities of H_2/CO lean (φ = 0.4 to φ = 1.0) premixed flames at different hydrogen fractions ranging from 0% to 100% at elevated pressure and room temperature was performed in a constant volume vessel using a Schlieren system. The unstretched laminar burning velocities were compared with data from the previous literature and simulated results. The results indicate that excellent agreements are obtained. The cellular instabilities of syngas-air flames were discussed and critical flame radii were measured. When hydrogen fractions are above 50%, the flame tends to be more stable as the equivalence ratio increases; however, the instability increases for flames of lower hydrogen fractions. For the premixed syngas flame with hydrogen fractions greater than 50%, the decline in cellular instabilities induced by the increase in equivalence ratio can be attributed to a reduction of diffusive-thermal instabilities rather than increased hydrodynamic instabilities. For premixed syngas flames with hydrogen fractions lower than 50%, as the equivalence ratio increases, the cellular instabilities become more evident because the enhanced hydrodynamic instabilities become the dominant effect. For premixed syngas flames, the enhancement of cellular instabilities induced by the increase in hydrogen fraction is the result of both increasing diffusive-thermal and hydrodynamic instabilities.

Keywords: premixed flame; syngas flame; intrinsic instabilities; critical flame radius

1. Introduction

With the increased energy demands and concerns about environmental protection, the development and the application of high efficiency clean combustion has attracted more and more attention. Lean mixture combustion has a number of positive features such as providing high thermal efficiency and reducing emissions [1–5]. Synthesis gas (syngas) has attracted significant interest in the field of energy and combustion as a promising alternative and an environmentally clean fuel [6,7]. Syngas primarily consists of H_2 and CO and can be derived from numerous sources. Syngas can be used in many power devices, such as gas turbines for integrated gasification combined cycle systems (IGCC) [8]. However, designing suitable combustors is a big challenge because of the significant variations in the composition of syngas due to the feedstock and gasification techniques [9]. Hence, the study of the fundamental combustion characteristics of H_2/CO premixed flames under different hydrogen fractions is important for further applications of syngas.

In a premixed flame, the appearance of cellular instabilities wrinkles the flame front and accelerates flame propagation, flame front instabilities may also contribute to the transition from deflagration to detonation [10]. The intrinsic instabilities of premixed flames are caused by hydrodynamic, diffusive-thermal, and body-force instabilities [11]. Hydrodynamic instability, which is caused by the expansion across the flame sheet [12,13], is present in all flames [14–16]. Diffusive-thermal instability, which is caused by the preferential diffusion of mass and heat [17,18], is only present in the flames with Lewis number (*Le*) < 1 [19–22]. Body-force instability, which is caused by the effect of buoyancy [23], is only apparent when the laminar propagation speed of the flame is low [24].

Up to now, a few studies have reported the cellular instabilities from experimental investigations; some scholars have studied the cellular instabilities of premixed hydrogen-air flames [25–29]. The cellular instabilities of mixtures of premixed hydrogen-hydrocarbon-air flames have also been studied by many scholars [30–35]. Nevertheless, studies about cellular instabilities of premixed syngas flames are relatively sparse, and most of the reported articles were mainly focused on cellular instabilities induced by the addition of inert gas or hydrocarbon under selected hydrogen fractions [36–40]. As a matter of fact, syngas is a blended fuel which mainly consists of H_2 and CO, so the cellular instabilities of syngas premixed flames are very complex due to the hydrogen fraction variation. To provide more information about the cellular instabilities of syngas premixed flame, this study focuses on lean and stoichiometric premixed H_2/CO/air flames as the research object to perform a systematic study on the cellular instabilities of syngas premixed flames under different hydrogen fraction conditions. The phenomena of cellular instabilities of lean premixed syngas flames have been observed at different hydrogen fractions (from 0% to 100%), equivalence ratios (φ, from 0.4 to 1.0) and elevated initial pressure of 0.3 MPa.

2. Experimental and Computational Specifications

2.1. Experimental Setups and Procedure

The experimental method used in this study is mainly composed of six parts: a closed combustion vessel, discharge system, ignition system, optical access system, high-speed camera and data acquisition and control system (Figure 1).

Figure 1. Schematic diagram of the experimental apparatus.

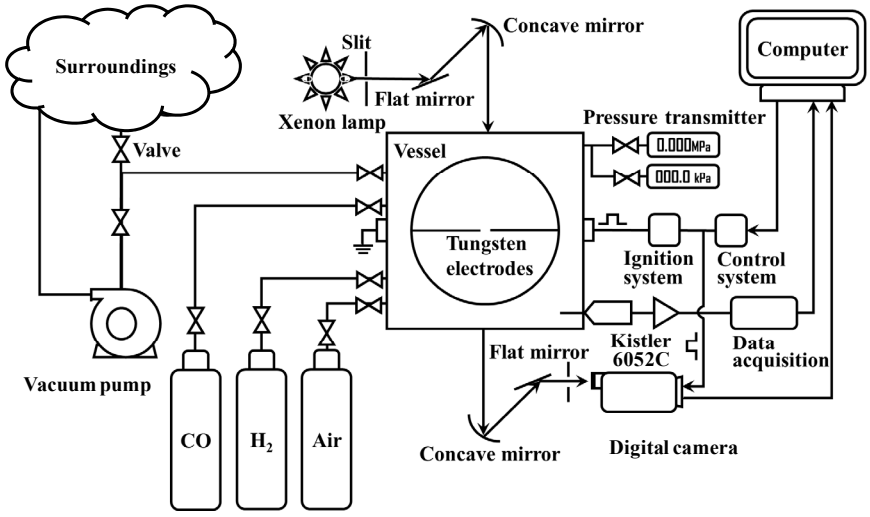

The closed combustion vessel is made of stainless steel and has a cubic inner chamber with a length of 140 mm. The 2-quartz windows of the vessel have effective diameters of 100 mm and are oppositely mounted. The discharge system includes five individual passages, namely, hydrogen bottle, carbon monoxide bottle, air bottle, vacuum pump and environment. The ignition system consists of a 12 V transistorized automotive ignition coil and a pair of tungsten–copper electrodes that are oppositely mounted on the two sides of the vessel other than the windows. The optical access system is Z-shaped and is mainly composed of one lamp, two flat reflectors, two slits and two concave mirrors with diameters of 200 mm and focal lengths of 2000 mm. The high-speed camera used is an IDT Motion Pro-Y4 (IDT, Newark, NJ, USA) operating at 10,000 frames per second with a resolution of 256 pixels × 256 pixels, the individual frame exposure is 3 μs with lamp power of 200 W. The data acquisition and control system mainly consists of two electrical pressure transmitters, one piezoelectric absolute pressure transducer associated with a charge amplifier and a data acquisition system. The two electrical pressure transmitters employed, namely, a DPA01M-P (with a band from −100.0 to 100.0 kPa) and DPA10M-P (with a band from −0.001 to 0.999 MPa), were produced by the Delta Group (Taiwan). The piezoelectric absolute pressure transducer is Kistler 6052C, and the discharge ampler is Kistler 5018A (Kistler, Winterthur, Switzerland). The synchronizer trigger employed is developed by the authors.

Procedurally, the vessel evacuated, and the mixture is prepared by adding hydrogen, carbon monoxide and air according to Dalton's law of additive pressure under the monitoring of the DPA01M-P and/or DPA10M-P units. The discharge process in the present investigation can be divided into the following stages: (i) the vessel is filled with hydrogen and carbon monoxide until the reading shown at the panel of the DPA01M-P has reached the desired value; (ii) the vessel is filled with air until the reading shown at the panel of DPA01M-P or DPA10M-P has reached the initial mixture pressure; (iii) once the desired mixture is prepared, 20 min is required to ensure the homogeneity and quiescence of the mixture. Finally, a control signal is sent to activate both the ignition system and high-speed camera synchronously, and the delay from the ignition to capture is set to 4 ms. The propagation of flame within the vessel is captured by the camera, whereas the variation of pressure on the inner wall of the vessel is recorded by the Kistler pressure transducer. Prior to refilling

for the next set of experiment, the vessel is flushed twice with dry air to remove any residual products. Thereafter, the vessel is evacuated again. In this study, the hydrogen is pure hydrogen with a purity of 99.995%, the carbon monoxide is pure carbon monoxide with a purity of 99.95% and the air is commercial grade compressed dry air with an oxygen-to-nitrogen volume ratio of 21:79.

In the study, at least three measurements have been performed at each condition for obtaining the average value. The initial pressure is measured by a pressure transmitter which accuracy is 0.001 MPa; the variation in initial pressure is 0.3 ± 0.001 MPa, so the relative error for the initial pressure is 0.3%. The high-speed camera is operated at 10,000 frames per second with a resolution of 256 pixels × 256 pixels, and the spatial resolution is 0.39 mm/pixel. The error bars in the figure reflects the corresponding standard deviations of laminar burning velocity and critical flame radius on the multi-times repeated experiments.

2.2. Laminar Burning Velocity

Within the closed combustion vessel, the premixed flame outwardly propagates spherically. The stretched flame propagation speed (S_b) can be derived from the data of flame radius *versus* time:

$$S_b = \frac{\mathrm{d}R}{\mathrm{d}t} \tag{1}$$

where R is the instantaneous flame radius and t is the elapsed time from the spark ignition. The flame propagation is affected by the electrodes when the flame is small, such as during the initial propagation period, and by the wall when the flame is sufficiently large, such as when constant pressure is absent in the spatial environment wherein the flame propagates. Thus, only flame radii between 6 [41] and 20 mm (about 0.3 times the radius of the wall [42]) are employed to avoid the aforementioned effects.

K is the temporal rate of the change of a flame surface element of area A:

$$K = \frac{\mathrm{d}(\ln A)}{\mathrm{d}t} = \frac{1}{A}\frac{\mathrm{d}A}{\mathrm{d}t} \tag{2}$$

K is defined as follows in the case of a spherically expanding laminar flame:

$$K = \frac{1}{A}\frac{\mathrm{d}A}{\mathrm{d}t} = \frac{1}{4\pi R^2}\frac{\mathrm{d}\left(4\pi R^2\right)}{\mathrm{d}t} = \frac{2}{R}\frac{\mathrm{d}R}{\mathrm{d}t} = \frac{2}{R}S_b \tag{3}$$

A linear relationship exists between the laminar flame propagation speed and K [43]:

$$S_b = S_b^0 - L_b \cdot K \tag{4}$$

where L_b is the Markstein length of burned mixtures and can be obtained as the negative value of the slope of the $S_b - K$ curve. S_b^0 is the unstretched flame propagation speed and can be considered the flame propagation speed without any stretch effect on the flame front; thus, S_b^0 can be obtained as the intercept value at $K = 0$.

During the initial propagation period, the flame can be considered to propagate under constant pressure. S_u^0 can be calculated from the mass conservation across the thin flame:

$$S_u^0 = S_b^0\left(\frac{\rho_b}{\rho_u}\right) \tag{5}$$

where ρ_b is the density of the burned mixture and ρ_u is the density of the unburned mixture calculated with the chemical equilibrium program GASEQ.

2.3. Thermal Expansion Ratio and Flame Thickness

Darrieus and Landau discovered that hydrodynamic instabilities are mainly caused by thermal expansion, which can be indicated by the thermal expansion ratio and flame thickness [26]. The thermal expansion ratio (σ) is defined as the ratio of unburned gas density to that of burned gas, which is calculated as:

$$\sigma = \rho_u / \rho_b \tag{6}$$

where ρ_u and ρ_b, the unburned and burned gas densities, respectively, can be obtained via thermodynamic calculation. The higher the density jump is, the stronger the destabilization becomes. Flame thickness (δ) can be determined by the temperature profile of the flame structure [40], which is calculated as:

$$\delta = \frac{T_{ad} - T_u}{(\mathrm{d}T / \mathrm{d}x)_{\max}} \tag{7}$$

where T_{ad} is the adiabatic temperature; T_u is the unburned gas temperature; and $(\mathrm{d}T/\mathrm{d}x)_{\max}$ is the maximum slope of the temperature profile. The $(\mathrm{d}T/\mathrm{d}x)_{\max}$ is determined using the premixed flame code PREMIX of the CHEMKIN-PRO package and the GRI3.0 Mechanism is used [44], since these where in close agreement with the present experimental laminar burning velocity data. With the decrease in flame thickness, the hydrodynamic instability increases due to the weaker influence of curvature and the enhanced intensity of induced baroclinic torque [26].

2.4. Lewis Number

The diffusive-thermal instability is caused by the competing effects of heat conduction and the reactant diffusion [45] and can always be quantitatively determined using the Lewis number (*Le*), which is defined as the ratio of the heat diffusivity to mass diffusivity of the deficient reactant to the abundant inert [46] and is used to describe diffusive-thermal instabilities, Le_{H2} and Le_{CO} can be calculated as expressed by the equation:

$$Le = \frac{\lambda / C_p}{\rho \cdot D} \tag{8}$$

where $\lambda / \left(C_p \cdot \rho\right)$ is the thermal diffusivity; C_p is the specific heat at constant pressure; λ is the heat conductivity; ρ is the density of the unburned mixture; and D is the mass diffusivity. For premixed syngas flames, two fuels exist in the reactants, and the Lewis number can thus be evaluated using the method by Law *et al.* [30], which is expressed as:

$$Le = 1 + \frac{q_{\mathrm{H_2}}(Le_{\mathrm{H_2}} - 1) + q_{\mathrm{CO}}(Le_{\mathrm{CO}} - 1)}{q} \tag{9}$$

where $q = q_{H2} + q_{CO}$ is the total heat release, with q_i (i refers to H_2 or CO) being the non-dimensional heat release associated with the consumption of species i, defined as $q_i = QY_i/C_pT_u$, where Q is the heat

of reaction; Y_i is the supply mass fraction of species i; c_p is the specific heat of the unburned gas; and T_u is the unburned gas temperature. Le_{H2} and Le_{CO} are the Lewis numbers of H_2-air mixture and CO-air mixture at φ_{H2} and φ_{CO}, respectively, where $\varphi_{H2} = (n_{H2}/n_A)/(n_F/n_A)st$, $\varphi_{CO} = (n_{CO}/n_A)/(n_F/n_A)_{st}$ are the H_2, and CO-based equivalence ratios, respectively, n_{H2}, n_{CO}, n_F, n_A are the mole fractions of H_2, CO, fuel and air in the reactant mixtures [33,37]. The diffusive-thermal instability is enhanced with the decrease of Lewis number [26].

3. Results and Discussion

3.1. System Validation and Laminar Burning Velocity

Published results of laminar burning velocities of H_2/CO/air mixtures at 0.3 MPa are lacking, but there are lots of published experiment data of laminar burning velocity with hydrogen fractions of 10% and 50% at 0.1 MPa.

To validate our experimental results, the additional laminar burning velocity of syngas/air mixtures at the pressure of 0.1 MPa has been measured and compared with previously published results. Figure 2 shows the measured laminar burning velocity of H_2/CO/air mixtures compared with those of previous studies [42,47–52]; all the data were measured with a spherically propagating flame at P_u = 0.1 MPa and all data are in good agreement. This proves the correctness of the data obtained in this investigation.

Figure 2. Comparison of measured unstretched laminar burning velocities and previously published results for 10%H_2-90%CO and 50%H_2-50%CO mixtures at P_u = 0.1 MPa.

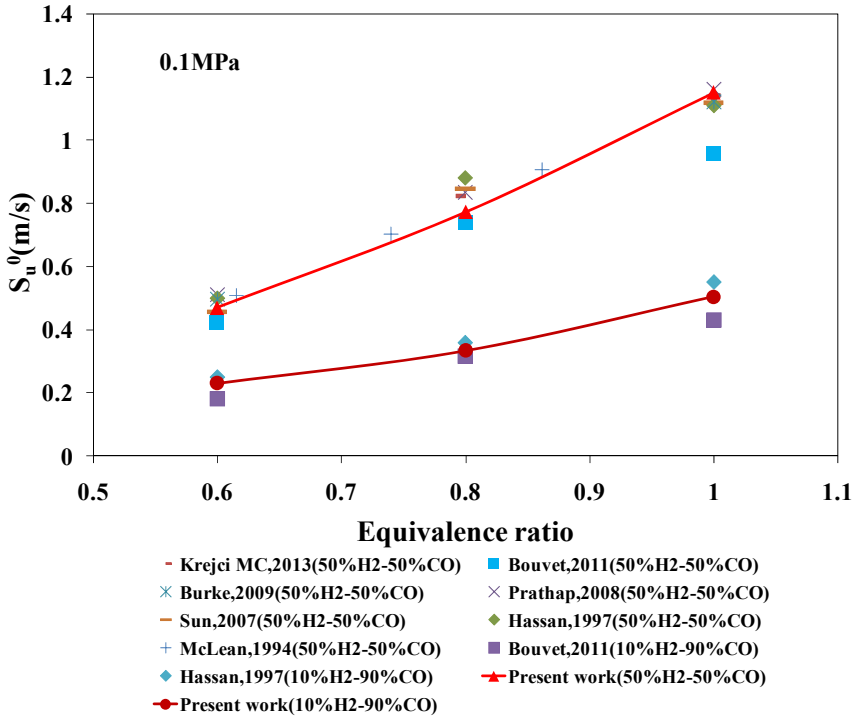

Figure 3 gives the unstretched laminar burning velocity *versus* hydrogen fraction for mixtures with various equivalence ratios at P_u = 0.3 MPa. The data of Park [39] for a 50%H_2/50%CO mixture at φ = 1.0 is also plotted in the figure and present work gives value consistent with Park's experimental

results. Simulations using the GRI Mesh 3.0 mechanism are also plotted in the figure and in general give good predictions on the unstretched laminar burning velocities of H_2/CO mixtures, although the predicted results are higher than the experimental results for some cases, so the mechanism is also used to ccalculate $(dT/dx)_{max}$ for getting the flame thickness. The unstretched laminar burning velocity of H_2/CO mixtures increases with increasing hydrogen fraction and equivalence ratio.

Figure 3. Unstretched laminar burning velocities of H_2/CO mixtures at P_u = 0.3 MPa.

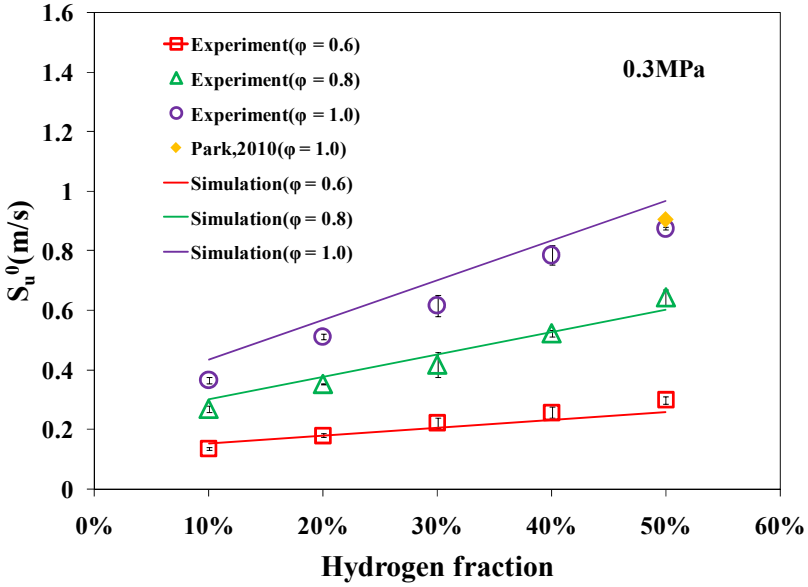

3.2. Flame Morphology

Figures 4 and 5 show the Schlieren images of premixed syngas-air flames with R = 20 mm with different hydrogen fractions and equivalence ratios, respectively. As shown in Figure 4, for the syngas premixed flame with φ = 0.4, the geometric centre of the flame was obviously lifted up from the initial position (namely, the ignition position) when the hydrogen fraction is below 50%, which means that the body-force instabilities are enhanced. Flames with lower hydrogen fractions show the body-force instabilities more evidently. With the increase of hydrogen fraction for all the equivalence ratios, more cells appear on the flame front. When the hydrogen fraction is higher than 50%, as shown in Figure 5, small cells become uniform over the entire flame front, which means the destabilisation propensity tends to be progressively promoted. From the observation, the cellular instability phenomena are obviously enhanced with the increase in hydrogen fraction for the same equivalence ratio. However, for the same hydrogen fraction, the effects of equivalence ratio on the variation of cellular instability vary. As shown in Figure 5, with hydrogen fractions above 50%, the flame tends to become more unstable with the decrease in equivalence ratio. This phenomenon is similar to seen for natural gas-hydrogen-air premixed flames reported by Huang *et al.* [35].

However, with hydrogen fractions below 50%, the flame tends to be more stable with the decrease in equivalence ratio, as shown in Figure 4. This observation has never been reported in any previous study.

Figure 4. Schlieren pictures for flames with hydrogen fractions from 10% to 50% at 0.3 MPa at different equivalence ratios for 20 mm radius.

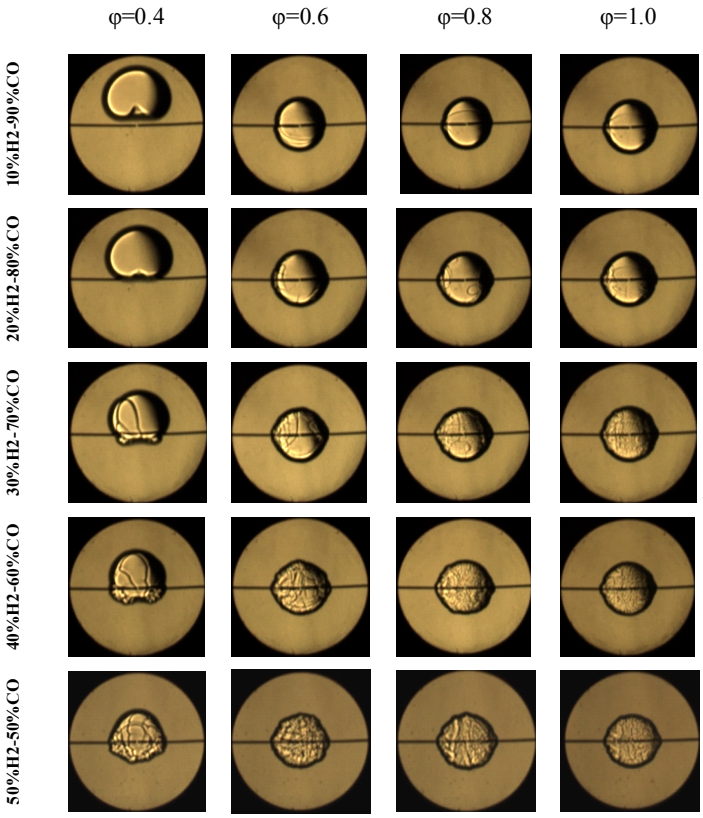

Figure 5. Schlieren pictures for flames with hydrogen fractions from 60% to 100% at 0.3 MPa at different equivalence ratios for 20 mm radius.

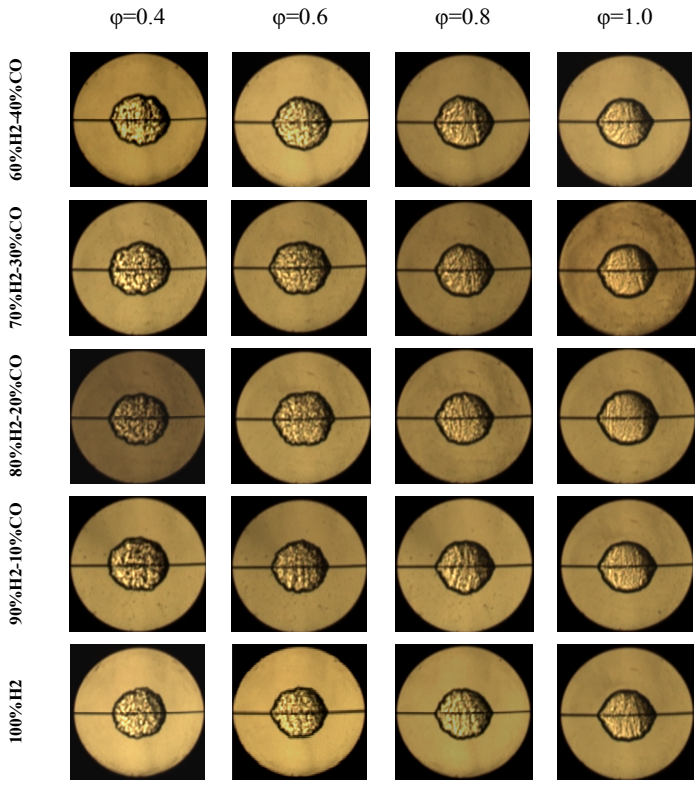

A detailed process of the propagation of the flames with hydrogen fraction of 30% is shown in Figure 6. For the premixed syngas flame with hydrogen fraction of 30% and φ = 0.4, several large cracks are induced by the ignition disturbances during the early propagation period, and those cracks continue to develop without branching as the flame further propagates. For the premixed syngas flame with φ = 0.6 to 1.0, the large cracks formed during the early propagation period become branched as the flame further propagates, and the phenomenon becomes more apparent at higher equivalence ratios. The flame tends to be more unstable with the increasing equivalence ratio. Instead, the cellular instabilities of syngas premixed flames decrease with the increase in equivalence ratio with the hydrogen fraction of 80%, as shown in Figure 7. To give a qualitative explanation, the parameters reflecting flame instability were calculated.

Figure 6. Schlieren pictures for flames of 30%H_2-70%CO at 0.3 MPa at different equivalence ratios for different radius.

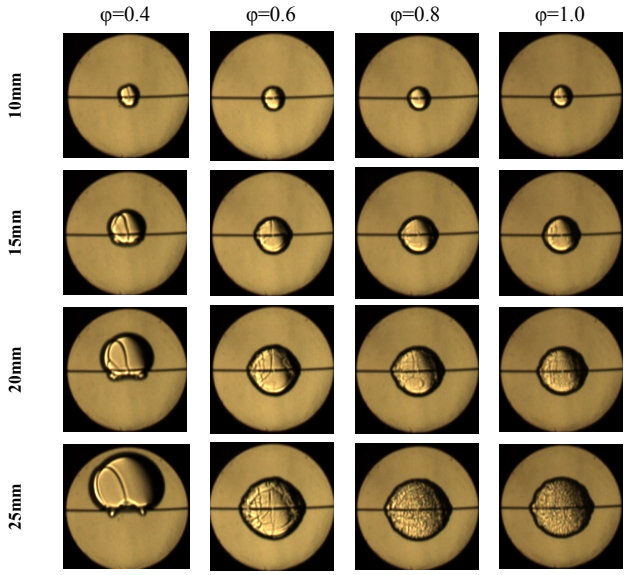

Figure 7. Schlieren pictures for flames of 80%H_2-20%CO at 0.3 MPa at different equivalence ratios for different radius.

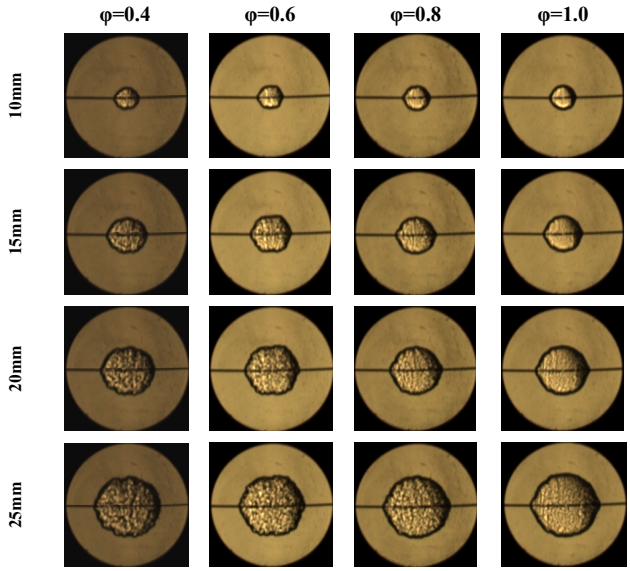

Figure 8 illustrates the variation in Lewis number with hydrogen fraction at different equivalent ratios at a pressure of 0.3 MPa. The Lewis number generally decreases with the increase in hydrogen fraction. The results indicate that the diffusive-thermal instability of lean syngas premixed flame is enhanced with the increase in hydrogen fraction. In addition, with the increase in equivalence ratio with hydrogen fractions less than 50%, the Lewis number nearly remains at the same value. For the premixed syngas flames with hydrogen fractions of more than 50%, the Lewis number at the same hydrogen fraction decreases with the decrease in equivalence ratio, which implies that the flame of low equivalence ratio is more unstable in terms of diffusive-thermal instability compared with the flame of relatively high equivalence ratio.

Figure 8. Lewis number plotted against hydrogen fraction.

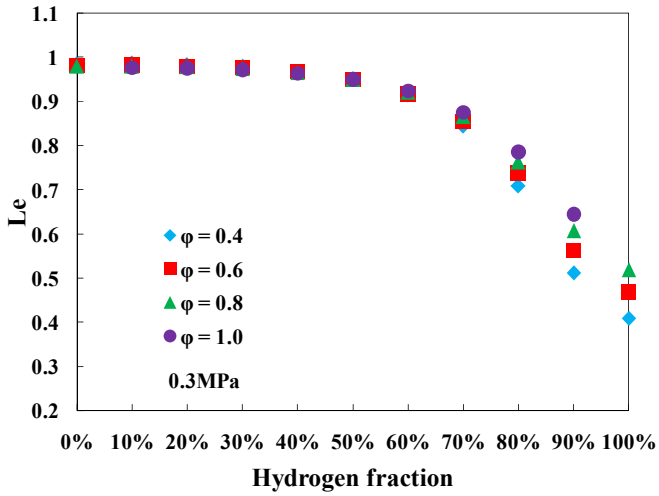

Figure 9 shows the flame thickness *versus* the hydrogen fractions for different equivalence ratios at 0.3 MPa. The flame thickness decrease significantly with the increase in hydrogen fraction and equivalence ratio. The decreased flame thickness results in an enhancement of the flame's destabilising propensity because of the weakened influence of curvature on the flame front as well as the strengthened baroclinic torque intensity, so the hydrodynamic instability is enhanced with the increase in hydrogen fraction and/or equivalence ratio for decreasing flame thickness.

Figure 9. Flame thickness plotted against hydrogen fraction.

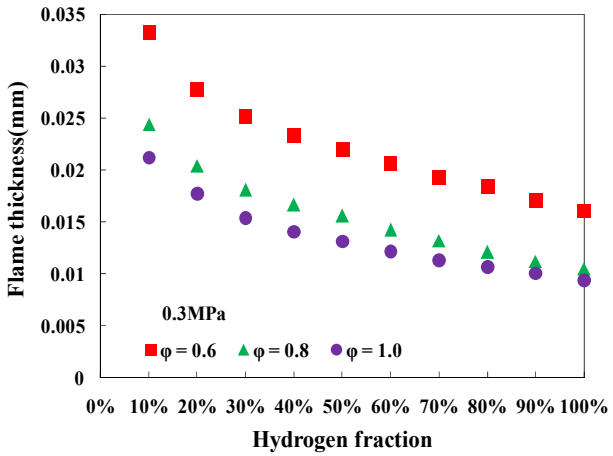

Figure 10 shows the thermal expansion ratio *versus* the hydrogen fractions for different equivalence ratios at 0.3 MPa. For a specific equivalence ratio, the thermal expansion ratio decreases inconspicuously with the increase in hydrogen fraction. In addition, for a specific hydrogen fraction, the thermal expansion ratio increases with the increase in equivalence ratio. The results indicate the hydrodynamic instability is enhanced with the increase in equivalence ratio. Based on the above discussions, for a specific hydrogen fraction, the hydrodynamic instabilities of syngas premixed flames are enhanced with the increase in equivalence ratio for both decreasing flame thickness and increasing thermal expansion ratio.

Figure 10. Thermal expansion ratio plotted against hydrogen fraction.

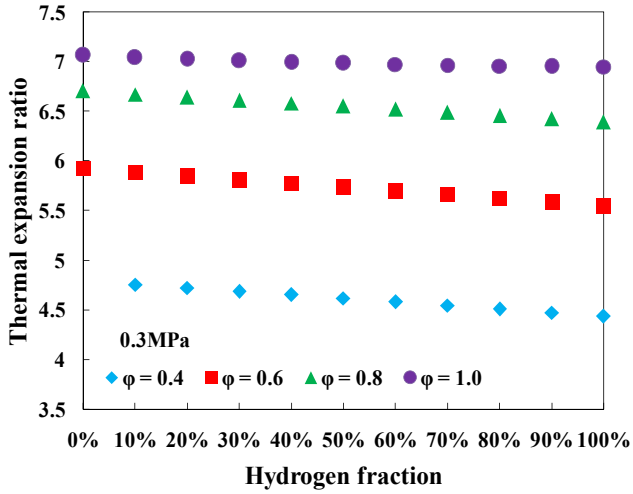

In general, when the hydrogen fraction is less than 50%, the enhancement of the cellular instabilities of the syngas premixed flame with the increase in equivalence ratio can be attributed to the dominant effect of the hydrodynamic instabilities. Furthermore, compared with the inconspicuous variation in thermal expansion ratio, the variation in flame thickness induced by the hydrogen fraction dominantly influences the intensity of hydrodynamic instabilities. At hydrogen fractions greater than 50%, the decline in the cellular instabilities induced by the increase of equivalence ratio can be attributed to the reduced diffusive-thermal instabilities rather than increasing hydrodynamic instabilities. With the increase in hydrogen fraction, the enhancement of the cellular instabilities of H_2/CO/air premixed flames results from the diffusive-thermal instability as the Lewis number decreases and the hydrodynamic instability as the flame thickness decreases.

3.3. Critical Flame Radius and Critical Peclet Number

During the initial flame propagation period, the cellular instabilities are suppressed by the strong stretch, and the suppressions decline and even extinguish as the flame expands. The "critical flame radius" (which is defined as the flame radius at which cells are smaller than the branched cracks and are no longer suppressed) has been employed to denote the onset of cellularity. As shown in Figure 11, the point at which the flame speed begins to accelerate rapidly with decreasing stretch defines a critical flame radius because the onset of cellularity is the primary reason of the self-acceleration of the flame [53,54].

Figure 11. Stretched flame speed *versus* stretch rate.

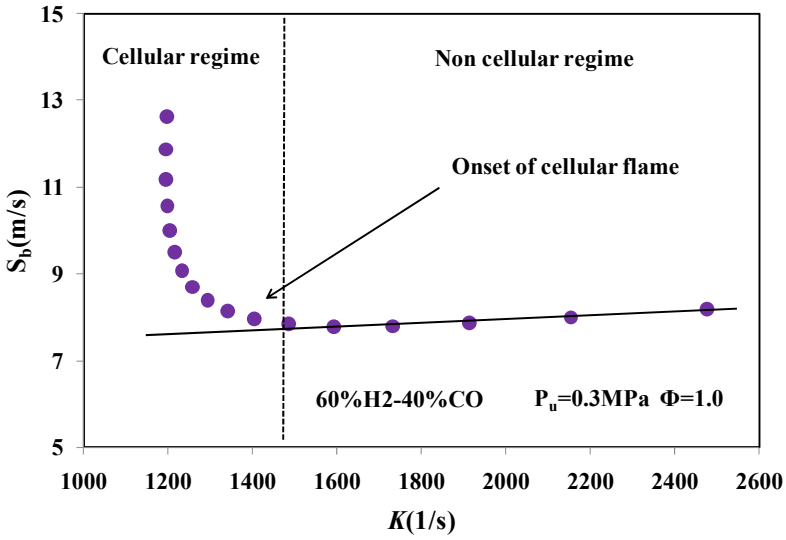

Figure 12 shows the critical flame radius *versus* the hydrogen fractions at different equivalence ratios. The data of Park [39] for a 50%H_2/50%CO mixture at φ = 0.8 and 1.0 is also plotted in the figure and the same trend is found. The critical flame radius evidently decreases with the increase in hydrogen fraction and increases with the increase in equivalence ratio at hydrogen fractions greater than 50%. However, the critical flame radius decreases with the increase in equivalence ratio at hydrogen fractions lower than 50%. This phenomenon is consistent with the observation of flame front photos.

Figure 12. Critical flame radius plotted against hydrogen fraction.

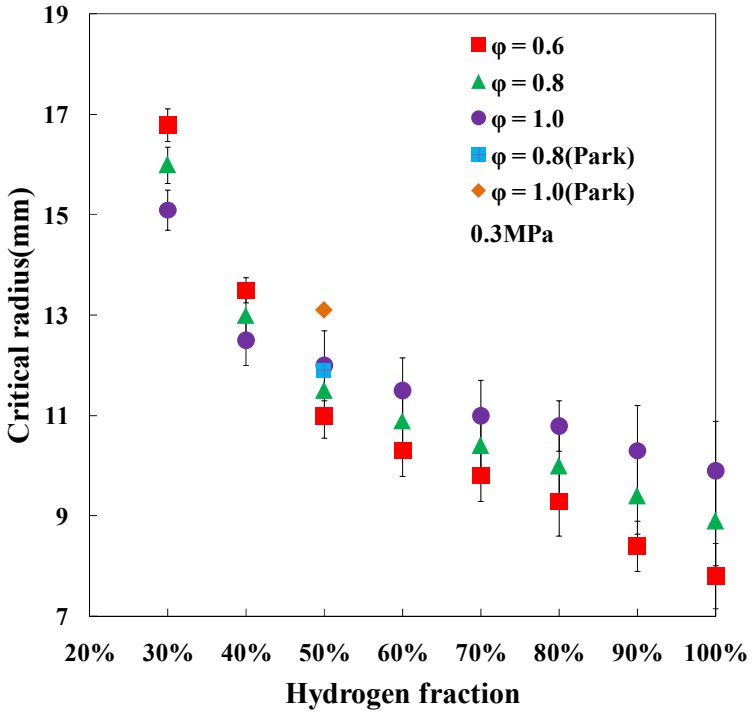

Critical Peclet number (Pe_{cr}), also representing the cellular instability, which is defined the ratio of critical flame radius to laminar flame thickness [55]. Figure 13 shows the critical Peclet number *versus*

the hydrogen fraction. Critical Peclet number is influenced by the combined effects of critical flame radius and flame thickness. The critical Peclet number decreases with the increase in hydrogen fraction at hydrogen fractions lower than 50%. However, with the increase in hydrogen fraction at hydrogen fractions greater than 50%, the critical Peclet number increases with equivalence ratios of 0.8 and 1.0, and the critical Peclet number changes little with an equivalence ratio of 0.6.

Figure 13. Critical Peclet number plotted against hydrogen fraction.

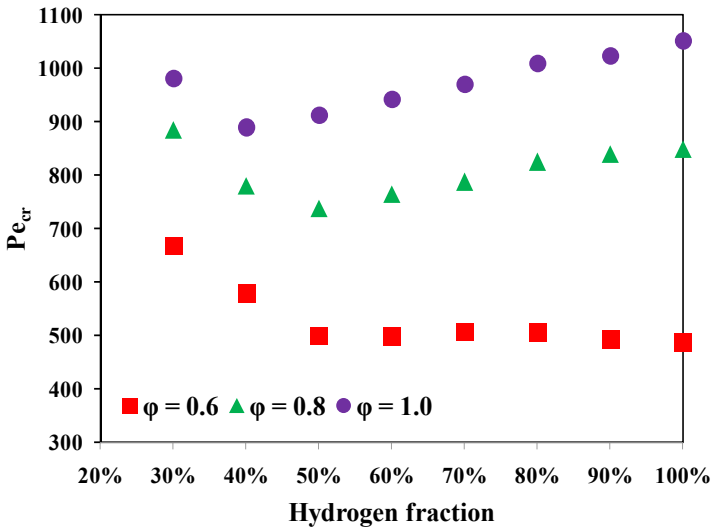

4. Conclusions

In the present work, the cellular instabilities of different hydrogen/carbon monoxide blends were studied using the outwardly propagating flame in a constant volume combustion bomb at elevated pressure and room temperature. The laminar burning velocities of syngas/air mixtures were measured and compared with previously published results and computed results and good agreements are obtained. The major conclusions of the study are as follows:

(1) When hydrogen fractions are above 50%, the flame tends to be more stable as the equivalence ratio increases; however, the instability increases for flames of lower hydrogen fractions.

(2) For the premixed syngas flames with hydrogen fractions lower than 50%, the effects of equivalence ratio on the variation in the Lewis number can be neglected. With the increase in equivalence ratio, the cellular instabilities become more evident because the enhanced hydrodynamic instabilities become the dominant effect.

(3) For the premixed syngas flame with hydrogen fractions greater than 50%, the decline in cellular instabilities induced by the increase in equivalence ratio can be attributed to the reducing diffusive-thermal instabilities rather than the increasing hydrodynamic instabilities.

(4) For the premixed syngas flame, the enhancement of cellular instabilities induced by the increase in hydrogen fraction is the result of both increasing diffusive-thermal and increasing hydrodynamic instabilities.

Acknowledgments

The present investigation is primarily supported by the Ph.D Programs Foundation of Ministry of Education of China (No. 20110009110023) and the Fundamental Research Funds for the Central Universities (No. M11JB00300).

Author Contributions

The author contributions list is as follows: Study concepts were proposed by Guo-Xiu Li and Hong-Meng Li. Literature research and study were designed by Hong-Meng Li and Guo-Xiu Li. Experimental studies and data acquisition were done by all the authors. Data analysis/interpretation and statistical analysis were done by Hong-Meng Li, Guo-Xiu Li, and Zuo-Yu Sun. Definition of the intellectual content of the manuscript, manuscript preparation and editing was made by Hong-Meng Li. Manuscript revision/review was made by Hong-Meng Li and Guo-Xiu Li. Manuscript final version was approved by Guo-Xiu Li.

Conflicts of Interest

The authors declare no conflict of interest.

References

1. Ji, C.; Wang, S. Combustion and emissions performance of a hybrid hydrogen–gasoline engine at idle and lean conditions. *Int. J. Hydrog. Energy* **2010**, *35*, 346–355.
2. Wang, J.; Huang, Z.; Tang, C.; Zheng, J. Effect of hydrogen addition on early flame growth of lean burn natural gas–air mixtures. *Int. J. Hydrog. Energy* **2010**, *35*, 7246–7252.
3. Yang, Z.Z.; Wang, L.; He, M.; Cao, Y. Research on optimal control to resolve the contradictions between restricting abnormal combustion and improving power output in hydrogen fueled engines. *Int. J. Hydrog. Energy* **2012**, *37*, 774–782.
4. Ji, C.; Wang, S.; Zhang, B. Combustion and emissions characteristics of a hybrid hydrogen–gasoline engine under various loads and lean conditions. *Int. J. Hydrog. Energy* **2010**, *35*, 5714–5422.
5. Yang, Z.; Wang, L.; Zhang, Q.; Meng, Y.; Pei, P. Research on optimum method to eliminate backfire of hydrogen internal combustion engines based on combining postponing ignition timing with water injection of intake manifold. *Int. J. Hydrog. Energy* **2012**, *37*, 12868–12878.
6. Burluka, A.A.; Ei-Dein Hussin, A.M.T.; Sheppard, C.G.W.; Liu, K.; Sanderson, V. Turbulent combustion of hydrogen-CO mixtures. *Flow Turbul. Combust*. **2011**, *86*, 735–749.
7. Fu, J.; Tang, C.L.; Jin, W.; Thi, L.D.; Huang, Z.; Zhang, Y. Study on laminar flame speed and flame structure of syngas with varied compositions using OH-PLIF and spectrograph. *Int. J. Hydrog. Energy* **2013**, *38*, 1636–1643.
8. Cormos, C.C. Evaluation of energy integration aspects for IGCC-based hydrogen and electricity co-production with carbon capture and storage. *Int. J. Hydrog. Energy* **2010**, *35*, 7485–7497.
9. Prathap, C.; Ray, A.; Ravi, M.R. Effects of dilution with carbon dioxide on the laminar burning velocity and flame stability of H_2-CO mixtures at atmospheric condition. *Combust. Flame* **2012**, *159*, 482–492.

10. Bradley, D.; Sheppart, C.G.W.; Woolley, R.; Greenhalgh, D.A.; Lockett, R.D. The development and structure of flame instabilities and cellularity at low Markstein numbers in explosions. *Combust. Flame* **2000**, *122*, 195–209.
11. Williams, F.A. *Combustion Theory*, 2nd ed.; Addison-Wesley: Redwood, CA, USA, 1985; p. 349.
12. Darrieus, G. Propagation d'un front de flame. *Tech. Mod*. **1938**, *30*, 18.
13. Landau, L.D. On the theory of slow combustion. *Acta Physicochim. URSS* **1944**, *19*, 77–88.
14. Mazaheri, K.; Mahmoudi, Y.; Radulescu, M.I. Diffusion and hydrodynamic instabilities in gaseous detonations. *Combust. Flame* **2012**, *159*, 2138–2154.
15. Hu, E.; Huang, Z.; He, J.; Zheng, J.; Miao, H. Measurements of laminar burning velocities and onset of cellular instabilities of methane-hydrogen-air flames at elevated pressures and temperatures. *Int. J. Hydrog. Energy* **2009**, *34*, 5574–5584.
16. Mukaiyama, K.; Shibayama, S.; Kuwana, K. Fractal structures of hydrodynamically unstable and diffusive-thermally unstable flames. *Combust. Flame* **2013**, *160*, 2471–2475.
17. Markstein, G.H. Cell structure of propane flames burning in tubes. *J. Chem. Phys.* **1949**, *17*, 428–429.
18. Manton, J.; von Elbe, G.; Lewis, B. Nonisotropic propagation of combustion waves in explosive gas mixtures and the development of cellular flames. *J. Chem. Phys.* **1952**, *20*, 153–157.
19. Kadowaki, S. The effects of heat loss on the burning velocity of cellular premixed flames generated by hydrodynamic and diffusive-thermal instabilities. *Combust. Flame* **2005**, *143*, 174–182.
20. Tang, C.L.; Huang, Z.H.; Jin, C.; He, J.; Wang, J.; Wang, X.; Miao, H. Laminar burning velocities and combustion characteristics of propane-hydrogen-air premixed flames. *Int. J. Hydrog. Energy* **2008**, *33*, 4906–4914.
21. Muppala, S.P.R.; Nakahara, M.; Aluri, N.K.; Kido, H.; Wen, J.X.; Papalexandris, M.V. Experimental and analytical investigation of the turbulent burning velocity of two-component fuel mixtures of hydrogen, methane and propane. *Int. J. Hydrog. Energy* **2009**, *34*, 9258–9265.
22. Bouvet, N.; Halter, F.; Chauveau, C.; Yoon, Y. On the effective Lewis number formulations for lean hydrogen/hydrocarbon/air mixtures. *Int. J. Hydrog. Energy* **2013**, *38*, 5949–5960.
23. Markstein, B.J. *Nonsteady Flame Propagation*; Pergamon: Oxford, UK, 1964; p. 49.
24. Kadowaki, S. The body-force effect on the cell formation of premixed flames. *Combust. Flame* **2001**, *124*, 409–421.
25. Tse, S.D.; Zhu, D.L.; Law, C.K. Morphology and burning rates of expanding spherical flames in H_2/O_2/inert mixtures up to 60 atmospheres. *Proc. Combust. Inst.* **2000**, *28*, 1793–1800.
26. Kwon, O.C.; Rozenchan, G.; Law, C.K. Cellular instabilities and self-acceleration of outwardly propagating spherical flames. *Proc. Combust. Inst.* **2002**, *20*, 1775–1789.
27. Sun, Z.Y.; Liu, F.S.; Bao, X.C.; Liu, X.H. Research on cellular instabilities in outwardly propagating spherical hydrogen-air flames. *Int. J. Hydrog. Energy* **2012**, *37*, 7889–7899.
28. Qiao, L.; Gu, Y.; Dahm, W.J.A.; Dahm, E.S.O.; Faeth, G.M. A study of the effects of diluents on near-limit H_2-air flames in microgravity at normal and reduced pressures. *Combust. Flame* **2007**, *151*, 196–208.
29. Hu, E.; Huang, Z.; He, J.; Miao, H. Experimental and numerical study on laminar burning velocities and flame instabilities of hydrogen–air mixtures at elevated pressures and temperatures. *Int. J. Hydrog. Energy* **2009**, *34*, 8741–8755.

30. Law, C.K.; Jomaas, G.; Bechtold, J.K. Cellular instabilities of expanding hydrogen/propane spherical flames at elevated pressures: Theory and experiment. *Proc. Combust. Inst.* **2005**, *30*, 159–167.
31. Law, C.K.; Kwon, O.C. Effects of hydrocarbon substitution on atmospheric hydrogen-air flame propagation. *Int. J. Hydrog. Energy* **2004**, *29*, 867–879.
32. Okafor, E.C.; Hayakawa, A.; Nagano, Y.; Kitagawa, T. Effects of hydrogen concentration on premixed laminar flames of hydrogen-methane-air. *Int. J. Hydrog. Energy* **2014**, *39*, 2409–2417.
33. Tang, C.; Huang, Z.; Wang, J.; Zheng, J. Effects of hydrogen addition on cellular instabilities of the spherically expanding propane flames. *Int. J. Hydrog. Energy* **2009**, *34*, 2483–2487.
34. Wu, X.; Huang, Z.; Wang, X.; Jin, C.; Tang, C.; Wei, L.; Law, C.K. Laminar burning velocities and flame instabilities of 2,5-dimethylfuran-air mixtures at elevated pressures. *Combust. Flame* **2011**, *158*, 539–546.
35. Miao, H.; Jiao, Q.; Huang, Z.; Jiang, D. Effect of initial pressure on laminar combustion characteristics of hydrogen enriched natural gas. *Int. J. Hydrog. Energy* **2008**, *33*, 3876–3885.
36. Song, W.S.; Jung, S.W.; Par, J.; Kwon, O.B; Kim, Y.J.; Kim, T.H.; Yun, J.H.; Keel, S.I. Effects of syngas addition on flame propagation and stability in outwardly propagating spherical dimethyl ether-air premixed flames. *Int. J. Hydrog. Energy* **2013**, *38*, 14102–14114.
37. Vu, T.M.; Park, J.; Kwon, O.B.; Kim, J.S. Effects of hydrocarbon addition on cellular instabilities in expanding syngas–air spherical premixed flames. *Int. J. Hydrog. Energy* **2009**, *34*, 6961–6969.
38. Hu, E.; Fu, J.; Pan, L.; Jiang, X.; Huang, Z.; Zhang, Y. Experimental and numerical study on the effect of composition on laminar burning velocities of H_2/CO/N_2/CO_2/air mixtures. *Int. J. Hydrog. Energy* **2012**, *37*, 18509–18519.
39. Vu, T.M.; Park, J.; Kwon, O.B.; Bae, D.S.; Yun, J.H.; Keel, S.I. Effects of diluents on cellular instabilities in outwardly propagating spherical syngas-air premixed flames. *Int. J. Hydrog. Energy* **2010**, *35*, 3868–3880.
40. Wang, J.; Huang, Z.; Kobayashi, H.; Ogami, Y. Laminar burning velocities and flame characteristics of CO-H_2-CO_2-O_2 mixtures. *Int. J. Hydrog. Energy* **2012**, *37*, 19158–19167.
41. Liu, C.C.; Shy, S.S; Chiu, C.W.; Peng, M.W.; Chung, H.J. Hydrogen/carbon monoxide syngas burning rates measurements in high-pressure quiescent and turbulent environment. *Int. J. Hydrog. Energy* **2011**, *36*, 8595–8603.
42. Burke, M.P.; Chen, Z.; Ju, Y.; Dryer, F.L. Effect of cylindrical confinement on the determination of laminar flame speeds using outwardly propagating flames. *Combust. Flame* **2009**, *156*, 771–779.
43. Bradley, D.; Hicks, R.A.; Lawes, M.; Sheppard, C.G.W.; Woolley, R. The measurement of laminar burning velocities and Markstein numbers for iso-octane–air and iso-octane–n-heptane–air mixtures at elevated temperatures and pressures in an explosion bomb. *Combust. Flame* **1998**, *115*, 126–144.
44. Smith, G.P.; Golden, D.M.; Frenklach, M.; Moriarty, N.W.; Eiteneer, B.; Goldenberg, M. GRI3.0 Mesh. Available online: http://www.me.berkeley.edu/gri_mech/ (accessed on 10 November 2013).
45. Liu, K.; Burluka, A.A.; Sheppard, C.G.W. Turbulent flame and mass burning rate in a spark ignition engine. *Fuel* **2013**, *107*, 202–208.
46. Moccia, V.; D'Alessio, J. Burning behaviour of high-pressure CH_4-H_2-air mixtures. *Energies* **2013**, *6*, 97–116.

47. Hassan, M.I.; Aung, K.T.; Faeth, G.M. Properties of laminar premixed CO/H/air flames at various pressures. *J. Propuls. Power* **1997**, *13*, 239–245.
48. Sun, H.; Yang, S.I.; Jomaas, G.; Law, C.K. High-pressure laminar flame speeds and kinetic modeling of carbon monoxide/hydrogen combustion. *Proc. Combust. Inst.* **2007**, *31*, 439–446.
49. Krejci, M.C.; Mathieu, O.; Vissotski, A.J.; Ravi, S.; Sikes, T.G.; Petersen, E.L. Laminar flame speed and ignition delay time data for the kinetic modeling of hydrogen and syngas fuel blends. *J. Eng. Gas Turbines Power* **2013**, *135*, 021503, doi:10.1115/1.4007737.
50. Prathap, C.; Ray, A.; Ravi, M.R. Investigation of nitrogen dilution effects on the laminar burning velocity and flame stability of syngas fuel at atmospheric condition. *Combust. Flame* **2008**, *155*, 145–160.
51. McLean, I.C.; Smith, D.B.; Taylor, S.C. The use of carbon monoxide/hydrogen burning velocities to examine the rate of the CO + OH reaction. *Symp. (Int.) Combust.* **1994**, *25*, 749–757.
52. Bouvet, N.; Chauveau, C.; Gökalp, I.; Halter, F. Experimental studies of the fundamental flame speeds of syngas (H_2/CO)/air mixtures. *Proc. Combust. Inst.* **2011**, *33*, 913–920.
53. Gu, X.J.; Haq, M.Z.; Lawes, M. Laminar burning velocity and Markstein lengths of Methane-air mixtures. *Combust. Flame* **2000**, *121*, 54–58.
54. Zamashchikov, V.V.; Alekseev, V.A.; Konnov, A.A. Laminar burning velocities of rich near-limiting flames of hydrogen. *Int. J. Hydrog. Energy* **2014**, *39*, 1874–1881.
55. Bechtold, J.K.; Matalon, M. Hydrodynamic and diffusion effects on the stability of spherically expanding flames. *Combust. Flame* **1987**, *67*, 77–90.